

RESEARCH ARTICLE

MICROSTRUCTURAL AND COMPOSITIONAL CHARACTERIZATION OF ROMAN BRONZE COINS FROM KHIRBAT EDH-DHARIH IN JORDAN

Abdulraouf Mayyas,¹ Wassef Al Sekhaneh,² Diya Al Fuqara,³ Ruba Seiseh,⁴ Fardous Al-Ajlouny,⁵ Zeidoun Al Muheisen,⁶ Jürgen Popp⁷

¹ Department of Conservation Science, Queen Rania Faculty of Tourism and Heritage, The Hashemite University, P.O. Box 330127, Zarqa 13133, Jordan; ² Department of Conservation and Management of Cultural Resources, Faculty of Archaeology and Anthropology, Yarmouk University, P.O. Box. 566, Irbid 21163, Jordan; ³ Department of Natural Resources and Chemical Engineering, Tafila Technical University, P.O. Box 179, Tafila 66110, Jordan; ⁴ Department of Cultural Resources Management and Conservation, School of Archaeology and Tourism, The University of Jordan, P.O. Box. 11942, Amman, Jordan; ⁵ Department of Sustainable Tourism, Queen Rania Faculty of Tourism and Heritage, The Hashemite University, P.O. Box. 330127, Zarqa 13133, Jordan; ⁶ Department of Archaeology, Faculty of Archaeology and Anthropology, Yarmouk University, P.O. Box 566, Irbid 21163, Jordan; ⁷ Leibniz Institute of Photonic Technology (IPHT) in Jena and the Chair of Physical Chemistry (IPC) at Friedrich Schiller University in Jena, Helmholtzweg 4, 07743 Jena, Germany

(✉ a_s_mayyas@hotmail.com)

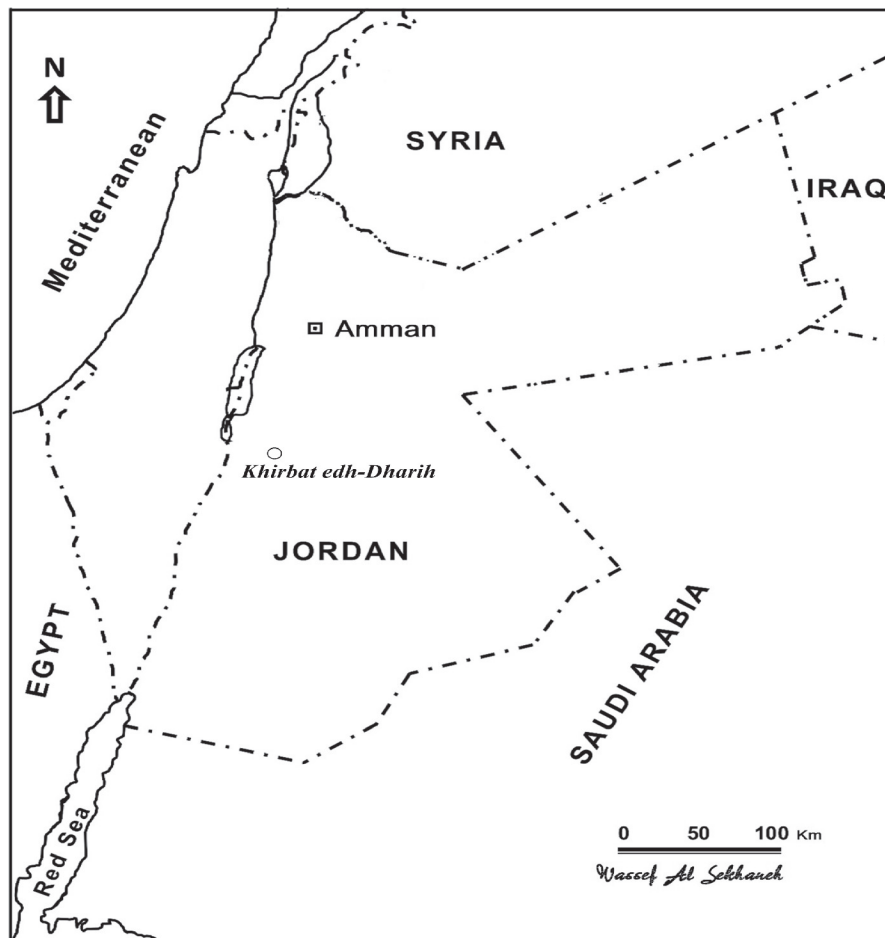


Figure 1. Map shows the location of *Khirbat edh-Dharikh* in Jordan.

Received: August 25, 2023. Modified: September 5, 2023. Accepted: September 11, 2023. Published: September 26, 2023.

Edited & Published by Pascual Izquierdo-Egea. English proofreading by Rachel Egan. Arqueol. Iberoam. Open Access Journal. License CC BY 3.0 ES. <https://n2t.net/ark:/49934/309>. <https://purl.org/aia/5208>.

ABSTRACT. *This study aimed at investigating the chemical and mineralogical compositions of five Roman coins (four copper-based and one silver-based alloys) corrosion products, and explore the topographic and morphological microscopic features of the patinas formed on the surface of the copper-based coins. For this purpose, an interdisciplinary approach to micro-destructive methods—microscopic (OM and SEM), mineralogical (XRD), elemental (XRF and SEM-EDX), and molecular (ATR-FTIR)—was conducted. The results showed that cuprite is the principle patina initially formed on the surface of the copper-based alloys by the redundant interaction with the surrounding environmental burial conditions, which is most likely an oxygenated and moisturized soil. This interaction was also observed in the formation of a secondary patina composed of malachite and azurite, which lately was invaded by the corrosive cycle process (bronze disease) represented by the formation of nantokite, atacamite and paratacamite that affected the cuprite primary patina of the copper-based coins during burial. The silver-based coin also suffered an aggressive attack by oxygen, sulfur and chloride ions during burial and formed oxide, sulfide, and chloride of silver, in addition to the corrosion products of cuprite, atacamite, and carbonate of copper, which is one of the alloying elements of this coin. The findings of this study also show that the copper-based coins were made of quaternary Cu-Sn-Zn-Pb alloy, and the silver-based coin was made of ternary Ag-Cu-Sn alloy. Therefore, the study points out that these coins were suffering from the corrosion phenomenon by the reaction with oxide, sulfide, carbonate, hydroxyl, and chloride ions, which are most likely found in the burial soil and incorporated within the alloy corrosion products. Contamination with Si, Fe, Al, and Ca elements present in the soil was also seen. We recommend protecting these alloys to prevent further degradation that may occur during storage and exposure to the atmosphere after excavation.*

KEYWORDS. *Khirbat edh-Dharib; Jordan; bronze; coin; corrosion; OM; SEM-EDX; XRF; XRD; ATR-FTIR.*

1. INTRODUCTION

Alloying copper with tin to form bronze began in the Near East by the end of the fourth millennium B.C., but only became widespread in the mid-third millennium B.C. (Akyuz *et al.* 2008; Roberts & Thornton 2014; Kaufman 2018). The term bronze generally refers to any alloy of copper that contains tin as the principal alloying element with or without other alloying metals such as zinc (Zn), lead (Pb), iron (Fe), aluminum (Al), manganese (Mn), silicon (Si) and nickel (Ni) (Thyssen Inc. 1998; McCafferty 2010; Kutz 2015). The main characteristics of the acquired alloy are usually good wear resistance, high hardness, corrosion resistance, good electrical conductivity, and good ductility (Collini 2012). However, objects made of copper and its alloys are subjected to the corrosion process forming various layers of products, some of which can be called patina. However, studying the chemical composition and properties of bronze objects and their corrosion products requires deep knowledge and attention due to the fact that copper and copper-based objects have various chemical and physical properties and because of the diverse nature of the surrounding environment before and after burial, as well as after excavation.

Generally, chemical compounds are always present in equilibrium with the surrounding environment, but a change in the environmental conditions will affect

their chemical compositions and/or quantities. This change can result from an alteration in the content of water, oxygen, and other gases, acid-base substances, pH, soluble salts, organic matter, and microorganisms. Therefore, when a copper-based (bronze) alloy object is exposed to the surrounding environment, copper-based oxides, hydroxides, sulfides, sulfates, carbonates, nitrates, chlorides, phosphates and others can produce. The kind of product that results depends on the type of reactive species present in the environment.

These products form through oxidation-reduction, acid-base, complexation, hydrolysis, ionic exchange and contamination processes (Sandu *et al.* 2008). They are formed at different stages in different environmental conditions during the object's lifetime forming different types of patinas over the metal alloy's surface. These corrosion stages comprise the 1) pre-burial stage (all ancient anthropogenic activities, including production and usage in ancient time), 2) burial and post-burial stages, where oxic and anoxic conditions are governed by oxygen and water content in the burial soil, as well as 3) during and after excavation stages (all anthropogenic activities, including the recovering, transporting, storage and laboratory manipulation processes).

The color of the corrosion layer depends on its chemical and physical properties. It is possible that one or more of these corrosion products may form the patina over the surface of the object. In particular, the cuprite

(Cu₂O, copper I oxide) forms in an aerated (oxic) and humid environment (Huisman *et al.* 2023). Almost all bronze objects can form primary cuprite layer in burial soil (Scott 2002; Oudbashi & Fadaei 2019; Oudbashi *et al.* 2019; Kotlar *et al.* 2020, 2021; Huisman *et al.* 2023). Cuprite produces in the initial stage of the corrosion and forms a primary orange-red-brown uniform coherent and compacted film of patina (depending on the impurities and the size of its particles), which efficiently isolates the underlying metal from the external environment and protect it from further deterioration under the same environmental conditions. Therefore, cuprite acts as a warning layer and is indicative of the initial corrosion interface between the metal and its environment (Scott 1997, 2002). Tenorite (CuO, copper II oxide) forms a dark gray color and it is insoluble in water; however, this compound is a rare copper corrosion product in most environments compared with cuprite, the most common corrosion product of copper (Scott 2002). This is because tenorite can be produced from the oxidation of cuprite and most copper corrosion products in the presence of oxygen in a thermodynamic process directional proportional to temperature (Evans 1976; Scott 2002; Huisman *et al.* 2023). Tenorite can also be produced from copper corrosion products, including malachite, azurite, and nanotokite, in a very alkaline environment (Gettens 1961; Scott 1997) or clean air with moisture, particularly, in the presence of chloride on the surface of the metal (Strandberg & Johansson 1998; Strandberg 1998; Petiti *et al.* 2020).

The thermodynamic spontaneous oxidation of cuprite to tenorite in an environment with calcareous property or with high carbon dioxide (CO₂) content was also highlighted by Doménech-Carbó *et al.* (2016, 2018) and Redondo-Marugán *et al.* (2017). Tenorite could be formed over the cuprite layer or possibly within the malachite and azurite copper corrosion products. Over the cuprite primary patina, however, a secondary patina could also be formed as a result of forming other copper corrosion products, such as green malachite and blue azurite (Kotlar *et al.* 2020; Huisman *et al.* 2023), as well as other products. Malachite and azurite form in the presence of carbon dioxide, water, and certain minerals, such as carbonate (Scott 2002; Oudbashi & Fadaei 2019; Kotlar *et al.* 2021; Huisman *et al.* 2023). They could be generated from copper metal or cuprite under these conditions (Oudbashi *et al.* 2019; Yang *et al.* 2020). The patina's color is also affected by the occurrence of other compounds, such as copper

sulfides or lead, which make it dark, while tin oxide or lead carbonate makes it more bright.

For its aesthetic characteristics and protection behavior, bronze patina is much appreciated in the art world (Canadian Chemical Processing 1975; Landolt 2007; Meigh 2018; Sandu *et al.* 2014; Mircea *et al.* 2009a, 2009b; Sandu *et al.* 2008; Catelli *et al.* 2018). However, when the chloride ion, which could exist either on the patina (e.g. pale green cuprous chloride, nanotokite, CuCl) or in the surrounding environment, interacts with moisture and oxygen (present in burial environment or in the air after recovering), a cyclic and self-sustaining degradation process commonly known as “bronze disease” is induced. In this process, the nanotokite will be ready for oxidation and hydrolysis producing hydrochloric acid and copper trihydroxychlorides (green Cu₂(OH)₃Cl): atacamite, clinoatacamite, botallackite, and the more complex polyanionic mineral paratacamite.



Hydrochloric acid can react with the copper ions present as corrosion products in the patinas and with the underlying un-corroded copper alloy, resulting in further cuprous chloride, which can repeat the degradation cycle in the oxic and humid environment until the whole copper of the object is consumed. Therefore, studying bronze objects and their corrosion products to determine whether they consist of chlorides, such as nanotokite or copper trihydroxychloride is a very essential and important step for protecting and conserving these objects. In bronze alloys, tin, the main alloying element, is also subjected to corrosion, particularly oxidation, by which Sn oxides (cassiterite, SnO₂, and stannous oxide, SnO) can be produced within the patina of ancient bronze objects.

This study presents important research in the field of corrosion of archaeological bronze coins (Cu alloys). The study investigates the copper corrosion patina to provide data for the conservators who will treat and preserve corroded bronze surfaces in the lab. It contributes to understanding the physical and chemical properties of these surfaces and, therefore, their preservation condition and conservation priority. There are many research interests focused on the patina of archaeological bronze objects (Scott 1994; Robbiola *et al.* 1998; Constantinides *et al.* 2002; Sandu *et al.* 2006; Chiavari *et al.* 2007; Bernard & Joiret 2009; Torrisi *et al.* 2010; Alberghina *et al.* 2011; Oudbashi *et al.* 2016; Vassiliou

Table 1. Front and back faces, weights, and dimensions of the five archaeological coins.

Sample	Image of coin	Characteristics
Coin (1)	 <p>The image shows the front and back faces of a dark, copper-based coin. The front face features a profile of a figure, and the back face shows a rectangular stamp with the word 'PROVIDENS' visible. A yellow ruler is placed to the right for scale, showing the coin's diameter is approximately 27.1 mm and its thickness is 2.7 mm.</p>	<p>Origin: Roman Weight: 19 g Diameter: 27.1 mm Thickness: 2.7 mm Material: Copper-based</p>
Coin (2)	 <p>The image shows the front and back faces of a silver-based coin. The front face depicts a profile of a figure, and the back face shows a profile of a figure. A yellow ruler is placed to the right for scale, showing the coin's diameter is approximately 25.1 mm and its thickness is 2.5 mm.</p>	<p>Origin: Roman Weight: 22 g Diameter: 25.1 mm Thickness: 2.5 mm Material: Silver-based</p>
Coin (3)	 <p>The image shows the front and back faces of a copper-based coin. The front face features a profile of a figure, and the back face shows a profile of a figure. A yellow ruler is placed to the right for scale, showing the coin's diameter is approximately 23.6 mm and its thickness is 2.1 mm.</p>	<p>Origin: Roman Weight: 13 g Diameter: 23.6 mm Weight: 2.1 mm Material: Copper-based</p>
Coin (4)	 <p>The image shows the front and back faces of a copper-based coin. The front face features a profile of a figure, and the back face shows a profile of a figure. A yellow ruler is placed to the right for scale, showing the coin's diameter is approximately 23.1 mm and its thickness is 2.0 mm.</p>	<p>Origin: Roman Weight: 22 g Diameter: 23.1 mm Thickness: 2.0 mm Material: Copper-based</p>
Coin (5)	 <p>The image shows the front and back faces of a copper-based coin. The front face features a profile of a figure, and the back face shows a profile of a figure. A yellow ruler is placed to the right for scale, showing the coin's diameter is approximately 23.1 mm and its thickness is 2.1 mm.</p>	<p>Origin: Roman Weight: 22 g Diameter: 23.1 mm Thickness: 2.1 mm Material: Copper-based</p>

et al. 2019). Above all, it is necessary to determine and understand the forms of corrosion products in bronze and to identify the types of patinas. This is because the patina protects the remaining metal part of the alloy. It is more than an inevitable natural phenomenon and it is very important from the points of view of conservation (NETPDC 1972; Scott 2002, 2011; Dillmann *et al.* 2014).

A large number of the metallic artifacts that were excavated in Jordan have existed in an unrealized state

of conservation. The problem is either due to a lack of interdisciplinary scientific collaboration, the degradation of the remains in their storage and other conservation factors. Therefore, the multidisciplinary approach in the archaeological research is essential. Without this approach, it would not be possible to extrapolate the knowledge of the past and preserve the cultural property for the future.

Depending on the multidisciplinary approach into studying the ancient artifacts, the use of various mi-

Table 2. The part of the coin artifact that was subjected to analysis.

Investigation Method	Targeted part of the coin	
	Corrosion Product	Bulk Metal
SEM-BSE	Yes	Yes
SEM-EDX	Yes	–
XRF	Yes	–
OM	Yes	–
XRD	Yes	–
FTIR	Yes	–

cro-destructive methods, such as optical microscopy (OM), scanning electron microscopy (SEM), and energy dispersive X-Ray (EDX), X-Ray fluorescence (XRF), X-Ray diffraction (XRD), and attenuated total reflection-Fourier transform infrared spectroscopy (ATR-FTIR), is essential to investigate the ancient metal objects found during archaeological excavations. Knowledge of the metallic material and its alteration should then allow the development of preventive or curative conservation based on understanding the properties of metal and its corrosions. These techniques, however, will be utilized in this study to investigate five Roman coins (four bronzes and one silver) and their corrosion products excavated at the site of *Khirbat edh-Dharib*.

2. THE SITE OF KHIRBAT EDH-DHARIH

Khirbat edh-Dharib is located on the King's Highway in the Wadi al-Laaban, a southern tributary of the Wadi al-Hesa, 12 km north of Tafileh and 7 km south of the high sanctuary of Khirbat et-Tannour, with which *Dharib* is closely associated. *Dharib* is a middle site in the countryside, 100 km north of Petra (Figure 1). It is located near the "King's Highway", the most important caravan route that connected the northern and southern parts of the Middle East, and the area does not lack water in abundance (Figure 1).

3. MATERIALS AND METHODS

Several copper alloys were discovered at the site of *Khirbat edh-Dharib* and identified as coin objects. This study aims to understand the properties of the chemical and physical corrosion processes of these finds. It investigates these artifacts with archaeometric capabil-

ity for applying interdisciplinary methods of bronze corrosion. Five full coin objects (Table 1) have complex corrosion on their surfaces resulting from the interaction of the objects with their environments during long-term burial. The methods of this study were applied to investigate the elemental and mineral compositions of these alloys and their corrosion products formed during the underground residence of ancient copper alloys dated to the Roman period. In addition, the "topography" and morphology of the complex-structured patina on the copper-based coins will be discussed. This is because these two properties change based on the copper alloy and the surrounding environment and, therefore, with the corrosion products and deposits on the surface. The five coins were photographed as shown in Table 1.

The microstructure of the corrosion products was investigated and characterized using OM and SEM. The mineral composition of the corrosion products was explored using XRD, whilst the elemental composition of the five coins' surface layers was investigated using XRF and SEM-EDX. However, the technique of EDX was mainly used to provide knowledge about the minor or amorphous corrosion products that are mainly not found by XRD. In addition, ATR-FTIR was used for further identification of the corrosion products based on the molecular bonding that existed in these products (Table 2).

X-Ray Fluorescence Analysis

XRF analysis was conducted for elemental identification. The *Tornado* spectrometer *M4 micro-XRF* (Bruker) was used for conducting the measurement; the side window of the X-ray tube was equipped with rhodium (Rh) that gives the poly capillary lens along with spot size, which focuses down to 25 μm consist of high intensity with the 15 μm which results in several pixels about

720 × 900. The time of 3 ms per pixel was noted for the measurement, and then every element requires a plotting time of about 2 hours which is considered as the total acquisition period.

SEM-EDX Analysis

The high-emission electronic microscope JSM-6300F was used to investigate, which was merged with a microprobe analyzer known as JXA-8800 (Jeol). The electron gun emitted the cold field, which is equipped with a system that contains an increased amount of brightness with high voltage operating at 30 kV. The device was combined with the type of detector known as *Everhart-Thornley*, which is used for the purpose of secondary electrons that are prepared by a YAG scintillator, which is a type of semiconductor used for backscattered electrons (BSE); they consist of energy-dispersive X-ray, a kind of spectrometer.

The mode of secondary electron (SE) that was ordinarily used by SEM micrographs is used more often for showing the samples of morphology and “topology” than it is used by backscattered electrons, which is a kind of mode for obtaining the contrast of composition. The average atomic numbers of higher elements show the region which is being contrasted with an increased amount of brightness. In contrast to this, a lighter species contains an area that is tendentially dark in appearance. For the identification of qualitative elements, the energy dispersive X-ray spectrometry was used. To this end, a type of detector was used, which is known as silicon drift detector (SDD), consisting of an *XFlash* of about 5010 (Bruker).

X-Ray Diffraction Analysis

For the identification of the mineral, the analysis of XRD was conducted; it consists of XRD *X'Pert* software that interface with PRO (Panalytical), which is being NI-filtered, and *Cuka* radiator that contains the wavelength about ($\lambda = 1.5405 \text{ \AA}$) was mainly used in almost all measurements. The type of X-ray diffractometer, known as *Shimadzu* XRD-6000, was used for analyzing the mineralogical composition along with the corrosion of products. The source that is provided for the purpose of the investigation is copper KL_{2,3} ($\alpha_{1,2}$) consisting of radiation about ($\lambda = 1.54178 \text{ \AA}$); it consists of a spectrum that acquired the energy of 40 kV with a measurement of scale around 2000 counts/min. The process of scanning determines the pattern from

20° to 70° 2 θ , consisting of a speed of 0.03° in a dual goniometer, which is operated at room temperature with an energy of 30 kV along with 10 mA. The high score software such as Panalytical's *X'Pert* was utilized for carrying out the identification of minerals. Each coin was scratched off from the surface along with a small amount of corrosion products, and it was then mixed and dispersed with the liquid ethanol for being fixed on a glass slide. When the ethanol was evaporated, the slide was introduced into the instrument of XRD of investigation.

Optical Microscopic analysis

To study the “topography” and morphology of the corrosion, a fine piercing saw was taken to every artifact from the edge of their cross sections. The cross-section was surrounded by an *Araldite*® 2020 consisting of epoxy resin. At room temperature, the time was cured for about 12 hours according to the setting, the samples were found in a pattern of silicon carbide paper *Sic* which range from 150 to 1200 grit (P150, P280, P400, P1200) which is then polished by a polisher *Buehler* which begins at 9–3 μm used mainly for polishing the alumina suspensions and decrease the highly polished surface that uses the pastes aluminum diamond. Ethanol was used for decontaminating the samples, which are finally at the drying stage. These samples were then studied by the polarized microscope.

ATR-FTIR Analysis

Using *Varian* 670-IR, the ATR-FTIR analysis was conducted with a limit of 4000–400 cm^{-1} along with a resolution of about 4 cm^{-1} . Analysis was carried out with attenuated total reflection (ATR) in a reflection mode which is prepared by germanium crystal (consist refractive index 4), and for each measurement, there is a collection of 64 scans.

4. RESULTS AND DISCUSSION

Corrosion products initially form on the surface of the bronze, but over time they create thick layers of corrosion products on top of the original metallic surface, and in some cases, they may penetrate the interior of the alloy. If the corrosion has not entirely consumed the bronze object, a core of un-corroded alloy may remain, surrounded by layers of corrosion products. In

Table 3. The elemental compositions of the five coins obtained by XRF.

Composition (wt %)	Sample no.				
	1	2	3	4	5
Cu	73.60	18.30	66.00	71.20	68.30
Sn	10.10	8.46	9.10	8.20	8.40
Zn	7.50	-	10.50	6.80	6.40
Pb	5.10	-	6.60	6.60	9.30
Al	-	0.30	5.50	5.50	5.50
Ag	-	71.00	-	-	-
Fe	3.60	1.34	1.80	1.40	1.60
Ca	0.10	0.60	0.50	0.30	0.50

this study, the XRF and EDX analyses were conducted on the patina of the five coins to determine the chemical composition of the corrosion layer and the alloy (from which elements the coins are made); however, they can provide indications of the elements present in the alloy in relevant percentages. XRF data are shown in Table 3, whilst EDX spectra are shown in figures 2 and 3.

The XRF data (Table 3) indicate that all the coin samples, except coin no. 2, are composed of quaternary (Cu-Sn-Zn-Pb) bronze basic composition. It is known that copper was alloyed with tin and zinc to increase the breaking strength and hardness, and with lead in order to improve castability and machinability. However, the data suggest that sample no. 2 is a silver coin alloyed with copper and tin.

SEM was utilized with the ordinary secondary electron (SE) mode to show the morphology and “topog-

raphy” of the sample and with the backscatter electron (BSE) mode to obtain a compositional contrast and characterize the metallographic structure of the uncorroded bronze using cross-sections taken from the coins. In BSE images, lighter shades correspond to regions with elements with higher average atomic numbers. Therefore, in un-corroded leaded tin bronzes, the lightest regions in the images typically have the greatest concentration of lead (Pb), while the darkest regions have a greater concentration of copper (Cu). Figures 4 and 5 show SEM-SE and SEM-BSE images of sample no. 1, which also represents samples no. 3 and 4, in which the edge of the un-corroded metallic core (bulk) and the two innermost corrosion layers are visible. This stratigraphic morphology of the patina of coin no. 1 (Figure 5) owns a sandwich structure in which the three layers—bulk copper, primary patina, and secondary patina—are discerned with some overlapping with each

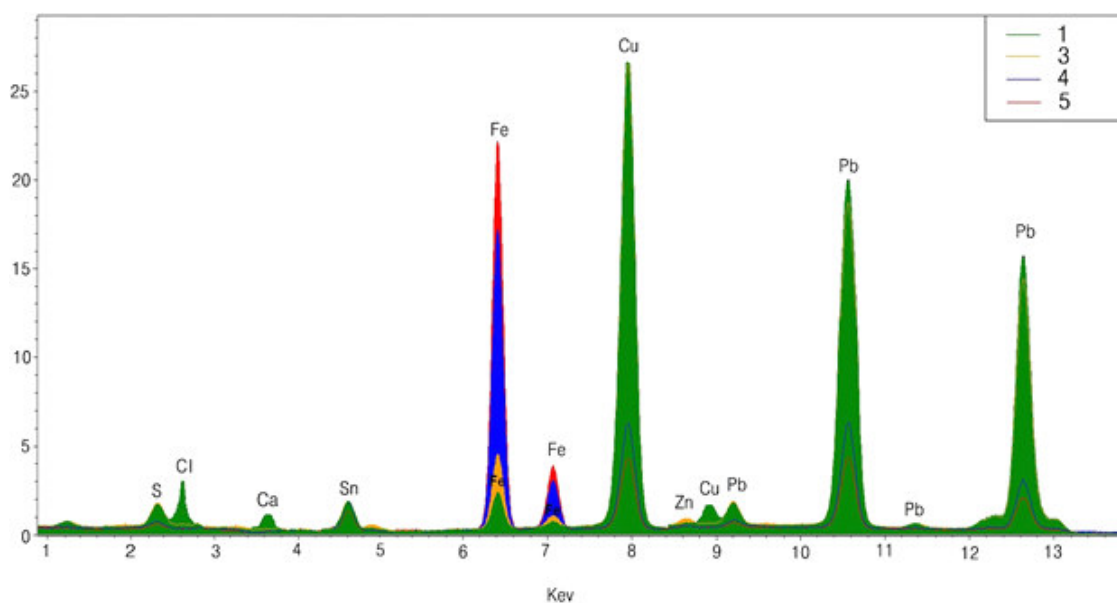


Figure 2. EDX elemental analysis of the corrosion products on the four bronze coins (no. 1, 3, 4, and 5).

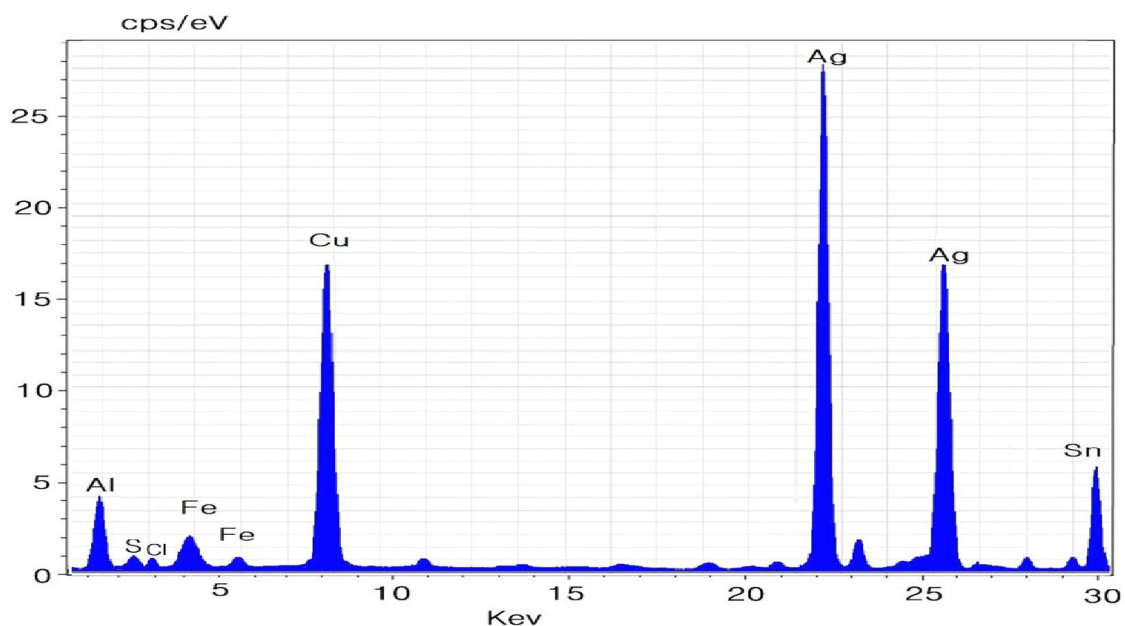


Figure 3. EDX elemental analysis of the corrosion products on the silver coin (no. 2).

other. The secondary patina appears with a surface “topography” that is irregular, fractured, and coarse (Figure 4). Further morphological investigation revealed that the white regions are Pb droplets. This segregated phase of Pb occurs when the copper alloy is cooled down to room temperature (Pb, with concentrations between 1 and 15% by weight in these samples, is essentially insoluble in bronze in the solid state and can therefore be considered separated from the bronze alloy).

Based on the above results, it was possible to verify that Roman coins no. 1, 3, 4, and 5 are made of bronze with quaternary composition of copper, tin, and lead (Cu-Sn-Zn-Pb). Coin no. 2, however, contains a high content of silver and lower amounts of copper and tin (Table 3); therefore, it represents a silver coin alloyed with copper and tin. A small amount of iron (Fe) was detected by XRF in the five alloys, with a content that varies up to 3.6 wt % (Table 3). Iron and aluminum could have come from the burial soil.

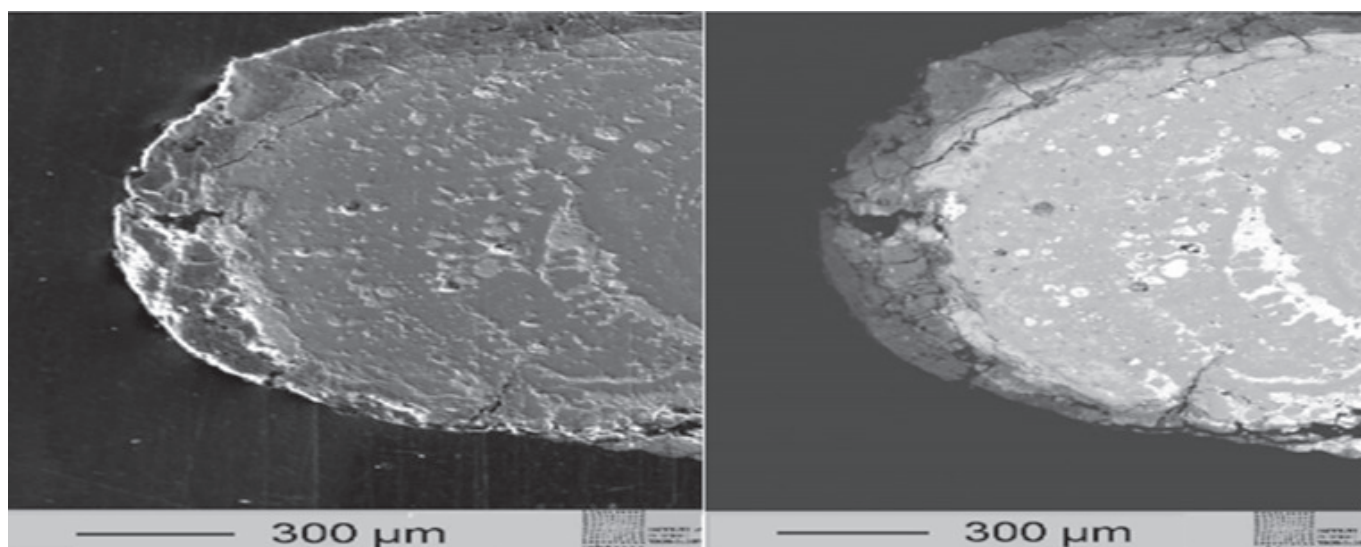


Figure 4. SEM images obtained in secondary electron (SE) mode (left) and backscatter electron (BSE) mode (right) of a cross-section taken from sample no. 1, which also represents samples no. 3 and 4. The left edges of both images show the outer corrosion layer on the surface, while the bulk of the alloy is shown upon moving from the internal border of the corrosion layer to the right in each image. The bright white points and patches are Pb droplets.

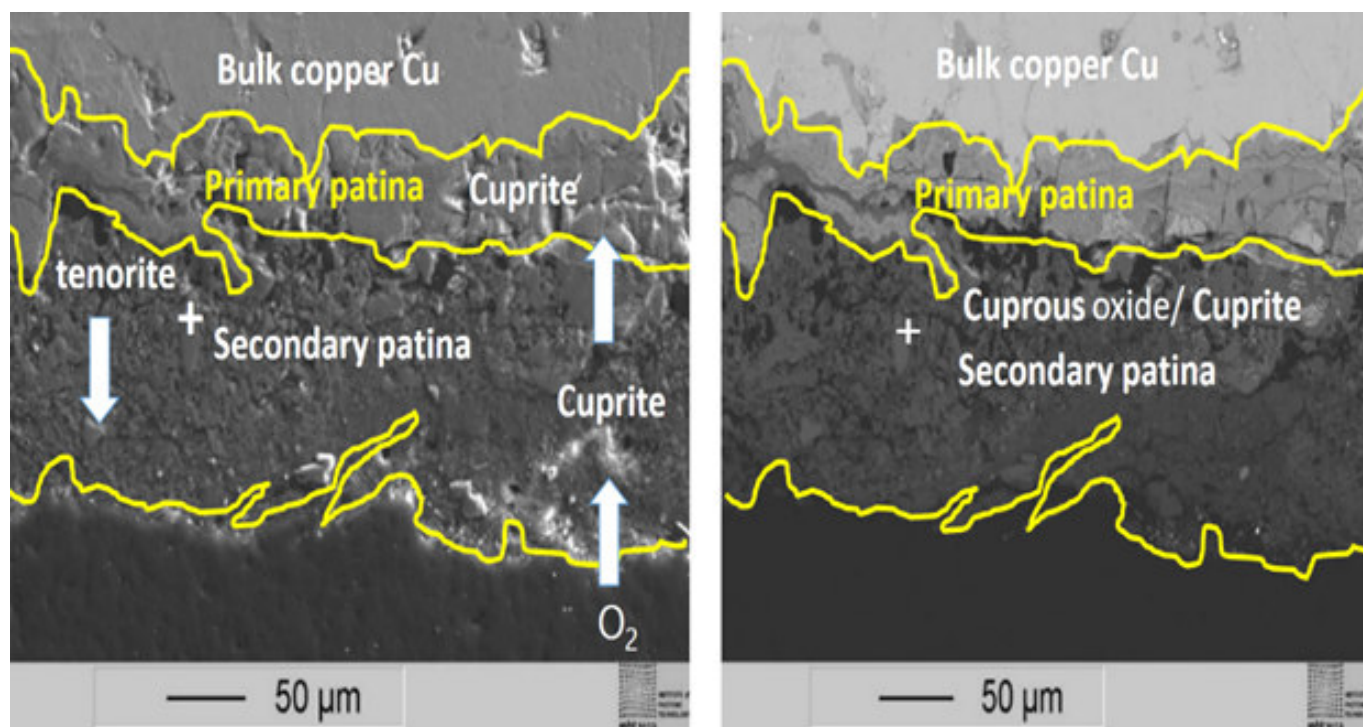


Figure 5. SEM images obtained in secondary electron (SE) mode (left) and backscatter electron (BSE) mode (right) of a cross-section taken from sample no. 1, which also represents samples no. 3 and 4. The images show the un-corroded metallic core (the bulk copper in the topmost region) and the first two corrosion layers (the primary and secondary patinas). The bright white points and patches are Pb droplets.

The SEM images displayed in Figure 6 represent a topographic view of an area of overlapping stress cracking networks that make up the corrosion crust on the surface of coin no. 5, which also represents coin no. 3.

The presence of copper chlorides in the corrosion crust is highlighted by the occurrence of chloride in the EDX spectra (Figure 2) and the presence of copper chloride-based compounds in the XRD spectra (Figure 7). It is

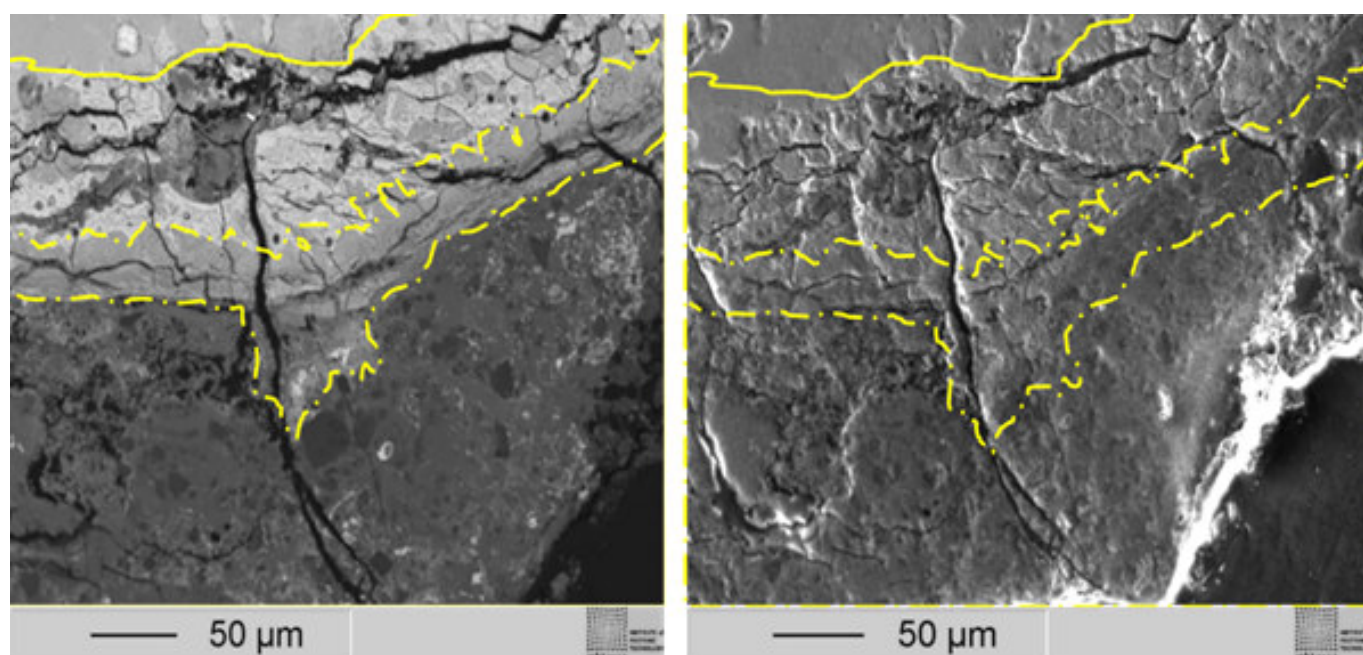


Figure 6. SEM images obtained in secondary electron (SE) mode (left) and backscatter electron (BSE) mode (right) of a cross-section taken from sample no. 5. The images show the un-corroded metallic core (the bulk copper in the topmost region) and the first two corrosion layers (the primary and secondary patinas). The bright white points and patches are Pb droplets, and the brightest areas are related to chlorides. The black bands in different directions are fissures and cavities as a result of the bronze disease.

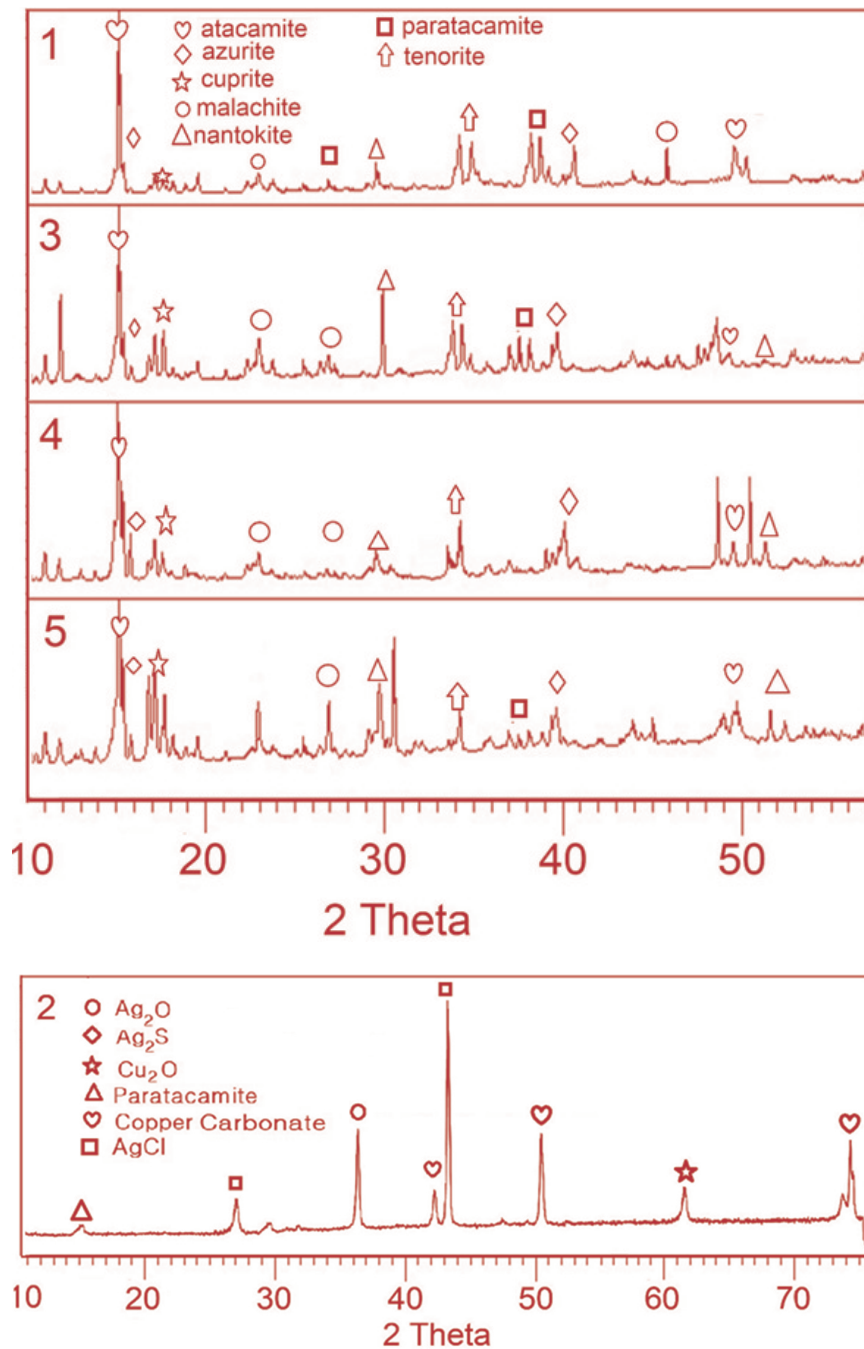


Figure 7. Bronze corrosion products identified by XRD on the surface of the copper alloys (samples no. 1, 3, 4, and 5) and silver alloy (sample no. 2).

noted that the areas in which chlorides are most present and penetrate the metal are the brightest in the image (Lopesino *et al.* 2018), which is shown in the backscattered electrons (BSE) image. It can be distinguished by the discontinuous surface topography with physical deterioration features, especially cracks, and pits, and by unevenly distributed corrosion products on the artifacts (Figure 6). XRD investigations were conducted on the patina products formed on the bronze coins af-

ter long-term burial in ancient soil (Figure 7). In addition, in order to understand the process of corrosion as proved by XRD (Figure 7), the corrosion products were also presented in Table 4 as observed under the optical microscope (Figure 8).

Based on their colors, different corrosion products on copper coins with various proportions can be identified in the photomicrographs (Figure 8). The red-brown patina is identified as cuprite, Cu_2O ; it is located

Table 4. Bronze corrosion products identified by XRD on the surface of the copper alloy objects.

Mineral/Corrosion Product	Formula	Color
Cuprite (Copper I oxide or cuprous oxide)	Cu_2O	dark red
Tenorite (Copper II oxide or cupric oxide)	CuO	gray black
Malachite Copper II dihydroxy carbonate	$\text{Cu}_2(\text{CO}_3)(\text{OH})_2$ or $\text{CuCO}_3\text{Cu}(\text{OH})_2$	green
Azurite Copper II dihydroxycarbonatet	$\text{Cu}_3(\text{CO}_3)_2(\text{OH})_2$ or $\text{Cu}_2(\text{CO}_3)_2\text{Cu}(\text{OH})_2$	blue
Nantokite (Copper I chloride or cuprous chloride)	CuCl	pale green
Atacamite Copper II trihydroxy chloride	$\text{Cu}_2(\text{OH})_3\text{Cl}$ or $\text{CuCl}_2 \cdot 3\text{Cu}(\text{OH})_2$ Orthorhombic crystal system	green
Paratacamite Copper II trihydroxy chloride	$\text{Cu}_2(\text{OH})_3\text{Cl}$ Rhombohedral crystal system	green to greenish-black

beneath the other patinas, in contact with the metal alloy. While the gray to black color is attributed to tenorite, the green patina (clearly shown in sample no. 5) is attributed to copper corrosion products called malachite (green $\text{Cu}_2\text{CO}_3(\text{OH})_2$), azurite (blue $\text{Cu}_3(\text{OH})_2(\text{CO}_3)_2$), nantokite (pale green CuCl), and both atacamite and paratacamite (green to greenish-black $\text{Cu}_2(\text{OH})_3\text{Cl}$).

In addition, the white patches could be attributed to corrosion products of lead, tin, and zinc alloying elements, and most probably to CaCO_3 from burial soil precipitated on the coins and participating in the formation of hydroxycarbonate corrosion products. Some elements can be deduced from the EDX and XRD spectra (figures 2 and 7), namely O, S, and Cl, which are most likely found in the burial soil and incorporated within the coins' corrosion patinas. O and Cl were structurally found in the corrosion layers as chemical compounds of copper (Figure 7 and Table 4). Many studies demonstrated that the most common copper corrosion compounds are oxides (cuprite and tenorite), hydroxylcarbonates (malachite and azurite), chlorides (nantokite), hydroxychlorides (atacamite and paratacamite), and hydroxysulfates (brochantite) (Scott 1997, 2002; Sandu *et al.* 2008, 2010; Oudbashi & Fadaei

2019; Petiti *et al.* 2020; Huisman *et al.* 2023). However, compounds with sulfur were not detected within the copper corrosion products but within the silver corrosion products (Figure 7).

When the bronze is left in contact with air, cuprite (dark red Cu_2O) film forms naturally on the bronze surface, which subsequently yields distinct corrosion products. It was demonstrated that tenorite (black CuO) can be produced from cuprite in an oxidizing environment by a thermodynamic process. On the other hand, malachite and azurite are two hydroxycarbonate copper corrosion products that can form an outer layer above the copper oxides in the presence of moisture and oxidizing conditions in burial soil with a pH value commonly between 6 and 10 (Huisman *et al.* 2023). This requires a carbonate source (Kotlar *et al.* 2020) like carbon dioxide (CO_2) and/or calcium carbonate (CaCO_3), etc.

Hydroxycarbonate products (malachite and azurite) may dissolve in an environment with pH value lower than 6. The formation of copper corrosion products in a calcareous (carbonate source) environment was pointed out by many authors (Bohnenkamp & Engell 1962; Scott 1997; Nair *et al.* 1999; Doménech-Carbó *et al.* 2014, 2016). Tenorite can also be produced from cop-

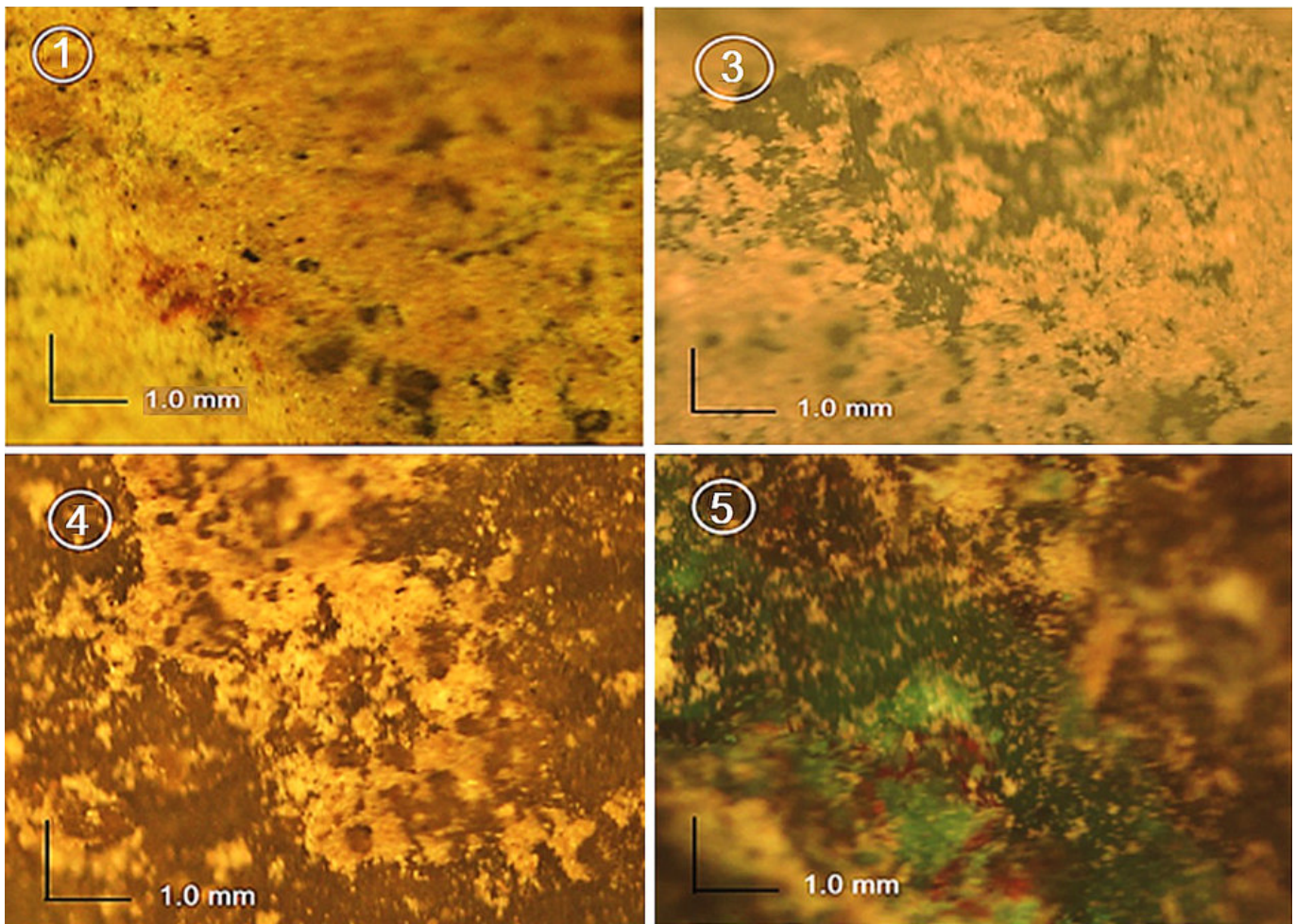


Figure 8. Optical microscopy of studied areas from four bronze coins (no. 1, 3, 4, and 5).

per corrosion products like malachite, azurite and nanokite in a very alkaline environment (Scott 1997), or cuprite in a calcareous medium or an environment with a high amount of CO_2 (Doménech-Carbó *et al.* 2014, 2016), as well as in clean moisturized air, particularly, in the presence of chloride on the surface of the metal (Strandberg & Johansson 1998). The occurrence of tenorite in the patina (Figure 7) may indicate that the coin was subjected to intentional or accidental heating over $300\text{ }^\circ\text{C}$, and this could have occurred in ancient times before burial. However, if tenorite formed in the burial soil then it could have originated from the other copper corrosion products in the presence of alkaline and carbonate medium. From the macroscopic and microscopic observation of some powdery light green/blue patinas located on the surface of the object, accompanied by the formation of small pitting, this phenomenon is known as “bronze disease” (Figure 8, clearly shown in samples no. 3 and 5).

The “bronze disease” is a cyclic phenomenon that repeats itself, producing aggressive activated irreversible

corrosion with a copper hydroxychloride product ($\text{Cu}_2(\text{OH})_3\text{Cl}$) caused by object interaction with chloride ions present in the burial soil (Bentahar *et al.* 2023; Monari *et al.* 2023; Pagano *et al.* 2023; Wang *et al.* 2023) and incorporated within the coins’ corrosion patinas. This is evident in figures 2, 6, 7, and 8. The light green color, obviously shown in sample no. 5, has been pitted as powdery spots called nanokite (CuCl) in a layer directly on the metallic surface (Figure 8). There are also two basic copper chlorides: atacamite and paratacamite (both have the same formula, $\text{Cu}_2(\text{OH})_3\text{Cl}$, but with different crystalline structures). They are detected in the powder accumulated in the pits of the “pitting” coin. The white spots are often embedded in, or layered above, the green and red patinas (Figure 8). It can be attributed to corrosion products of lead, tin and zinc originally present in the copper alloy, and possibly to carbonate, precipitated as calcium carbonate from burial soil.

On the other hand, it is known that silver objects are also affected by O, S, and Cl compounds that exist

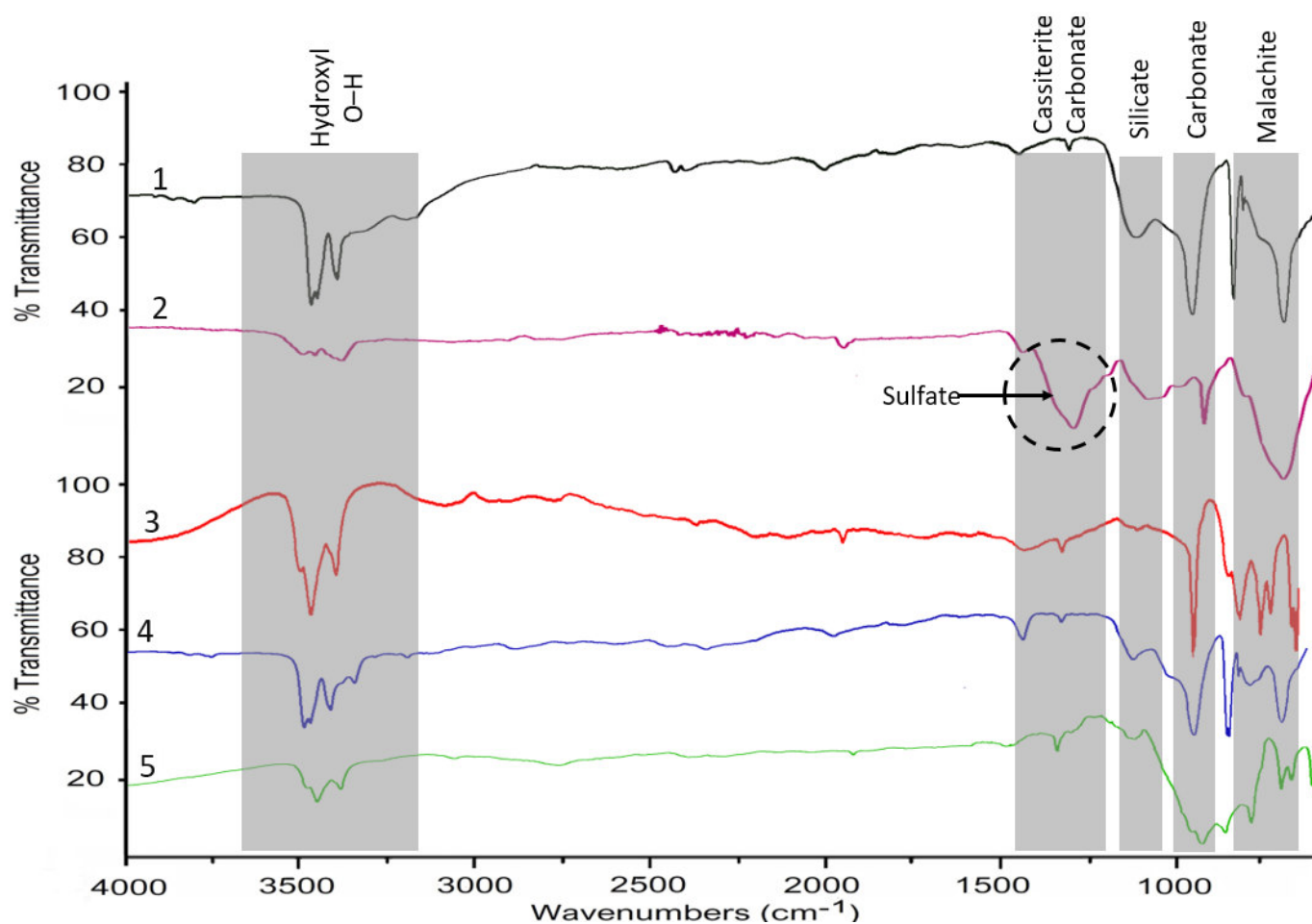


Figure 9. ATR-FTIR spectra (4000–500 cm^{-1}) collected on the coin patina of the five samples no. 1-5.

in the soil and form silver oxide (Ag_2O) corrosion product as a protective coating layer. This passive surface loses its defensive property when sulfur and chloride ions are present, and in this case corrosion products, mainly silver sulfide (Ag_2S), silver sulfate (Ag_2SO_4), and silver chloride (AgCl) are formed. The formation of Ag_2S may continue to destruct the silver coin completely (Pieta *et al.* 2018). However, among these silver corrosion products, AgCl is the most frequently detected compound in silver objects found at archaeological sites (Pieta *et al.* 2018). In addition, cuprite (Cu_2O) and litharge (PbO) can be formed as corrosion products of Cu and Pb when these metals are present within the silver alloy (Doménech-Carbó *et al.* 2018; Pieta *et al.* 2018). EDX spectrum informs the existence of sulfur and chlorine elements in the corrosion layer of the silver alloy (Figure 3).

XRD investigation, however, revealed the occurrence of silver corrosion products— Ag_2O , Ag_2S , and AgCl —as well as the copper corrosion products, Cu_2O , CuCO_3 (copper carbonate) and $\text{Cu}_2(\text{OH})_3\text{Cl}$ (paratacamite), in the alloy no. 2 (Figure 7). The formation of these cop-

per corrosion products indicates that the coin could have been subjected to an aggressive corrosion condition. Lead II oxide (PbO , litharge) was not seen in XRD, XRF, or EDX data, indicating that the silver most probably was alloyed with Cu and Sn elements to form the ternary (Ag-Cu-Sn) alloy no. 2. To increase the mechanical characteristics silver was frequently alloyed with copper (Marchand *et al.* 2014).

As shown in the optical microscopic image (Figure 8), sample no. 5 has a surface with an obvious green color. SEM examination of the sample revealed a distorted surface (Figure 6) and the XRD analysis revealed the mineral composition, including the two copper hydroxyl carbonates, malachite and azurite (Figure 7), suggesting the presence of carbonate in the copper corrosion products of the sample.

FTIR spectra of carbonate show four peaks of normal vibrational modes (Figure 9): ν_1 for C–O symmetric stretching, ν_2 for O–C–O out-of-plane bending, ν_3 for C–O asymmetric stretching, and ν_4 for O–C–O in-plane deformation bending (Chiavari *et al.* 2006; Bilinski 2008; Wu & Wang 2019; Kotlar *et al.* 2021). The

FTIR signals in the range of 1450–1250 cm^{-1} in the samples are signals for carbonate and sulfate. Given that FTIR can be used to distinguish between different phases of calcium carbonate (Malvault *et al.* 1995; Frost *et al.* 2002; Wang *et al.* 2010), the signal at 1486 cm^{-1} suggests that calcium carbonate exists in the samples as vaterite. The existence of peaks at 742 cm^{-1} and 880 cm^{-1} (Malvault *et al.* 1995) confirms this. In addition, the presence of calcium carbonate may be confirmed by the appearance of Ca as shown in the XRF data (Table 3) and EDX spectra (Figure 2). All these observations suggest that the green surface is attributed to malachite, a carbonate-based degradative product. Malachite, $\text{Cu}_2\text{CO}_3(\text{OH})_2$, is also present, as evidenced by several peaks. The two bands at 1092 and 1030 cm^{-1} are assigned to the two C–O stretching vibrations, symmetric and asymmetric, respectively.

While the two bands at 877 cm^{-1} and 819 cm^{-1} correspond to the two bending modes of malachite carbonates, out-of-phase and in-phase, respectively (Frost *et al.* 2002; Frost & Dickfos 2007; Buzgar & Apopei 2009). All these observations support the copper carbonate corrosion products in the four copper-based coins but are seen in sample no. 5.

FTIR reflectance spectroscopy can be used to identify the different basic copper II salts that form on copper when it corrodes. However, the O–H stretching mode region (nearly above 3250 cm^{-1}) cannot be used because the FTIR signals of different compounds overlap significantly in these parts of the spectra (Figure 10).

Based on XRF analyses, sample no. 1 has the greatest tin content (10.1%) of all the surface samples analyzed (Table 3). Tin is typically present as a corrosion byproduct on ancient metals in the form of cassiterite, SnO_2 (tin IV oxide). Cassiterite is exceedingly difficult to define as a corrosion product due to its properties. Additionally, it is frequently coated by other corrosion products, making it challenging to identify the peaks in an FTIR spectrum that are attributed to SnO_2 . The FTIR spectra of the samples revealed many peaks in the fingerprint region (Figure 9).

The spectra displayed a peak at 820 cm^{-1} , which is related to the vibrations of metal-oxide stretching (Kotlar *et al.* 2021), namely Sn–O and Cu–O stretching (Kotlar *et al.* 2021). Cassiterite is commonly identified by two peaks around 678 cm^{-1} in FTIR spectra (Frost *et al.* 2013) (Figure 10). The presence of SnO_2 is proved by the peak at 786 cm^{-1} . The band appears at around 1050–1150 cm^{-1} informing the existence of Si-oxides. In addition, the peak at 1092 cm^{-1} , which was

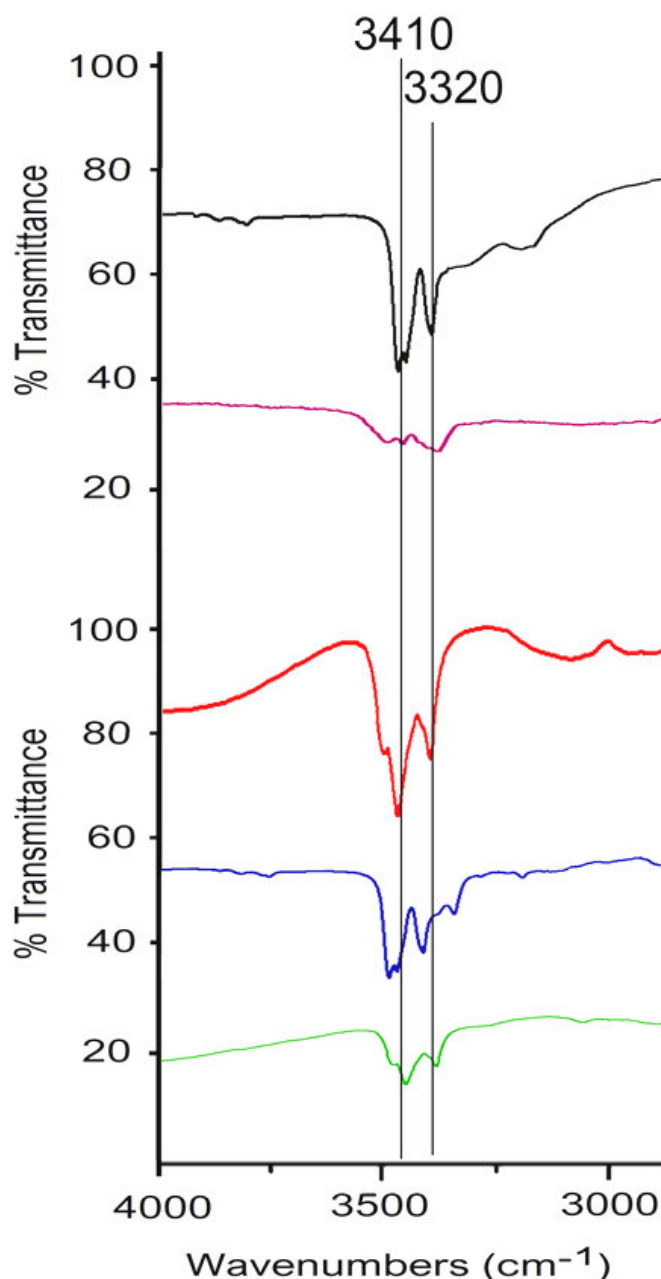


Figure 10. ATR-FTIR spectra (4000–2750 cm^{-1}) collected on the coin patina of the five samples no. 1-5.

ascribed to the carbonate compound, possibly malachite, is also related to Si–O. Silicates, such as quartz (SiO_2) and carbonate, such as calcite (CaCO_3) are usually soil minerals present in the burial environment (Brassard *et al.* 2004; Buzatu & Buzgar 2010).

According to XRF and EDX analyses, the five samples included a small amount of iron. Fe_2O_3 is anticipated to exist on the surface. However, if it was not created during bronze production, then at least it was deposited from sediments during burial. The majority of Fe–O bands appear below 600 cm^{-1} (Volpi *et al.* 2023). The peaks related to sulfate copper corrosion

products, such as posnjakite ($\text{Cu}_4\text{SO}_4(\text{OH})_6 \cdot \text{H}_2\text{O}$), antlerite ($\text{Cu}_3(\text{SO}_4)(\text{OH})_4$), or brochantite ($\text{Cu}_4\text{SO}_4(\text{OH})_6$), were not seen in the FTIR spectra of the copper-based alloys.

An FTIR signal for sulfate appeared in the silver alloy (sample no. 2) in the range of $1450\text{--}1250\text{ cm}^{-1}$, which was previously located for carbonate (Figure 9). In addition, the internal vibrational modes of sulfate ions are shown in the FTIR spectra at 880 cm^{-1} . XRD results indicated the presence of silver sulfide but not sulfate. It is therefore presumed that sample no. 2 contains sulfate in an inorganic form deposited on the surface of the object rather than a sulfate copper corrosion product resulting from the reaction of sulfur with the silver of the object. In this sample, however, copper carbonate and paratacamite were detected in the XRD spectrum (Figure 7). Carbonate is approved by the FTIR carbonate C–O broadband within the range of $1462\text{--}1430\text{ cm}^{-1}$. While the copper hydroxyl chloride product (paratacamite, $\text{Cu}_2(\text{OH})_3\text{Cl}$) could be discerned by the O–H stretching band that appears approximately within the range of $3350\text{--}3450\text{ cm}^{-1}$ and the O–H bending modes that appears between $810\text{--}950\text{ cm}^{-1}$ (Yu *et al.* 1999).

5. CONCLUSION

Bronze and silver coin artifacts were found at the archaeological site of *Khirbat edh-Dharib* and dated to the Roman period. They were subjected to different micro-destructive analyses using different analytical techniques as an integrated approach for this study. The investigations revealed that the basic alloying metals are quaternary Cu-Sn-Zn-Pb system in the case of the copper-based coins and ternary Ag-Cu-Sn system in the

case of the silver-based coin. The metal alloys were subjected to degradative corrosion processes during the long period of burial in the soil leading to different levels of degradative corrosions.

These alloys interacted with O^{2-} , S^{2-} , CO_3^{2-} , OH^- , and Cl^- ions present in the burial soil; therefore, these ions incorporated within the alloy corrosion products. On the other hand, Si, Fe, Al, and Ca elements were also detected in these corrosion layers and were considered burial soil contaminants.

The degree of degradation reached an aggressive corrosive level in case of some of these samples, in which the “topographical” and morphological features of the corrosion layers were explored. The XRF scanning using *Bruker M4 Tornado Micro-XRF* instrument is recommended for deeper investigation in order to obtain comprehensive bulk and surface analyses of the samples. Finally, we also recommend that action take place to prevent the further destruction of the coins after excavation, particularly, methods to reduce corrosion induced by chloride and sulfide ions which are particularly destructive.

Acknowledgments

The researchers are grateful to the research group of Prof. Jürgen Popp at the Leibniz Institute of Photonic Technology (IPHT) in Jena and the Department of Physical Chemistry at Friedrich Schiller University in Jena for the SEM, SEM-EDX, and FTIR measurements, and to the FH Münster University of Applied Sciences for the XRF measurements, as well as to the Yarmouk University, laboratories of the Faculty of Archaeology and Anthropology, for the OM and XRD measurements.

REFERENCES

- AKYUZ, S.; T. AKYUZ; S. BASARAN; C. BOLCAL; A. GULEC. 2008. Analysis of ancient potteries using FT-IR, micro-Raman and EDXRF spectrometry. *Vibrational Spectroscopy* 48(2): 276–280.
- ALBERGHINA, M.F.; R. BARRACO; M. BRAI; T. SCHILLACI; L. TRANCHINA. 2011. Integrated analytical methodologies for the study of corrosion processes in archaeological bronzes. *Spectrochimica Acta Part B: Atomic Spectroscopy* 66(2): 129–137.
- BENTAHAR, M.; A. PETITMANGIN; C. BLANC; A. CHABAS; S. MONTRESOR; C. NICLAEYS; A. ELBARTALI; D. NAJJAR; R. DUCCINI; M. JEAN; S. NOWAK; R. PIRES-BRAZUNA; P. DUBOT. 2023. Does Atmospheric Corrosion Alter the Sound Quality of the Bronze Used for Manufacturing Bells? *Materials* 16(13): 4763.
- BERNARD, M.C.; S. JOIRET. 2009. Understanding corrosion of ancient metals for the conservation of cultural heritage. *Electrochimica Acta* 54(22): 5199–5205.

- BILINSKI, H. 2008. Weathering of sandstones studied from the composition of stream sediments of the Kupa River (Croatia). *Mineralogical Magazine* 72(1): 23–26.
- BOHNENKAMP, K.; H.J. ENGELL. 1962. Ablauf der Oxydation von Eisen und Kohlenstoff bei der Verzunderung von Eisen-Kohlenstoff-Legierungen. *Archiv für das Eisenhüttenwesen* 33(6): 359–367.
- BRASSARD, D.; D.K. SARKAR; M.A. EL KHAKANI; L. OUELLET. 2004. High-*k* titanium silicate thin films grown by reactive magnetron sputtering for complementary metal-oxide-semiconductor applications. *Journal of Vacuum Science & Technology A* 22: 851–855.
- BUZATU, A.; N. BUZGAR. 2010. The Raman study of single-chain silicates. *Analele Stiintifice de Universitatii “Al. I. Cuza” din Iasi. Seria Geologie* 56(1): 107–125.
- BUZGAR, N.; A.I. APOPEI. 2009. The Raman study of certain carbonates. *Analele Stiintifice de Universitatii “Al. I. Cuza” din Iasi. Seria Geologie* 55(2): 97–112.
- CANADIAN CHEMICAL PROCESSING. 1975. Southam Business Publications.
- CATELLI, E.; G. SCIUTTO; S. PRATI; Y. JIA; R. MAZZEO. 2018. Characterization of outdoor bronze monument patinas: the potentialities of near-infrared spectroscopic analysis. *Environmental Science and Pollution Research* 25: 24379–24393.
- CHIAVARI, C.; A. COLLEDAN; A. FRIGNANI; G. BRUNORO. 2006. Corrosion evaluation of traditional and new bronzes for artistic castings. *Materials Chemistry and Physics* 95(2–3): 252–259.
- CHIAVARI, C.; K. RAHMOUNI; H. TAKENOUTI; S. JOIRET; P. VERMAUT; L. ROBBIOLA. 2007. Composition and electrochemical properties of natural patinas of outdoor bronze monuments. *Electrochimica Acta* 52(27): 7760–7769.
- COLLINI, L., ED. 2012. *Copper Alloys: Early Applications and Current Performance. Enhancing Processes*. IntechOpen.
- CONSTANTINIDES, I.; A. ADRIAENS; F. ADAMS. 2002. Surface characterization of artificial corrosion layers on copper alloy reference materials. *Applied Surface Science* 189(1–2): 90–101.
- DILLMANN, P.; G. BÉRANGER; P. PICCARDO; H. MATTHIENSEN. 2014. *Corrosion of Metallic Heritage Artefacts: Investigation, Conservation and Prediction of Long Term Behaviour*. Elsevier.
- DOMÉNECH-CARBÓ, A.; M.T. DOMÉNECH-CARBÓ; S. CAPELO; T. PASÍES; I. MARTÍNEZ-LÁZARO. 2014. Dating Archaeological Copper/Bronze Artifacts by Using the Voltammetry of Microparticles. *Angewandte Chemie International Edition* 53(35): 9262–9266.
- DOMÉNECH-CARBÓ, A.; S. CAPELO; J. PIQUERO; M.T. DOMÉNECH-CARBÓ; J. BARRIO; A. FUENTES; W. AL SEKHANEH. 2016. Dating archaeological copper using electrochemical impedance spectroscopy. Comparison with voltammetry of microparticles dating. *Materials and Corrosion* 67(2): 120–129.
- DOMÉNECH-CARBÓ, A.; M.T. DOMÉNECH-CARBÓ; J. REDONDO-MARUGÁN; L. OSETE-CORTINA; J. BARRIO; A. FUENTES; M.V. VIVANCOS-RAMÓN; W. AL SEKHANEH; B. MARTÍNEZ; I. MARTÍNEZ-LÁZARO; T. PASÍES. 2018. Electrochemical Characterization and Dating of Archaeological Leaded Bronze Objects Using the Voltammetry of Immobilized Particles. *Archaeometry* 60(2): 308–324.
- EVANS, V.R. 1976. *The Corrosion and Oxidation of Metals (Second Supplementary Volume)*. London: E. Arnold.
- FROST, R.L.; M.J. DICKFOS. 2007. Raman spectroscopy of halogen-containing carbonates. *Journal of Raman Spectroscopy* 38(11): 1516–1522.
- FROST, R.L.; W.N. MARTENS; L. RINTOUL; E. MAHMUTAGIC; J.T. KLOPROGGE. 2002. Raman spectroscopic study of azurite and malachite at 298 and 77 K. *Journal of Raman Spectroscopy* 33(4): 252–259.
- FROST, R.L.; Y. XI; R. SCHOLZ; A. LÓPEZ; F.M. BELOTTI. 2013. Vibrational spectroscopic characterization of the phosphate mineral hureaulite – $(\text{Mn, Fe})_5(\text{PO}_4)_2(\text{HPO}_4)_2 \cdot 4(\text{H}_2\text{O})$. *Vibrational Spectroscopy* 66: 69–75.
- GETTENS, R. J. 1961. Mineral alteration products on ancient metal objects. *Studies in Conservation* 6(sup. 1): 89–92.
- HUISMAN, H.; R. ACKERMANN; L. CLAES; L. VAN EIJCK; T. DE GROOT; I. JOOSTEN; F. KEMMERS; N. KERKHOVEN; J.W. DE KORT; S.L. RUSSO *ET ALII*. 2023. Change lost: Corrosion of Roman copper alloy coins in changing and variable burial environments. *Journal of Archaeological Science: Reports* 47: 103799.
- KAUFMAN, B. 2018. Anthropology of Metallurgical Design: A Survey of Metallurgical Traditions from Hominin Evolution to the Industrial Revolution. In *Metallurgical Design and Industry*, eds. B. Kaufman & C. Briant, pp. 1–70. Cham: Springer.
- KOTLAR, M.; N. MATIJAKOVIĆ; V. DESNICA; K. MARUŠIĆ. 2021. Studying a 2 millennia old bronze kettle using easily accessible characterization techniques. *Heritage Science* 9: 10.
- KOTLAR, M.; N. MATIJAKOVIĆ; V. DESNICA; K. MARUŠIĆ. 2020. Using characterization techniques for determining the history of a 2 millennia old kettle made of bronze alloyed with iron. *Research Square*, Preprint (Version 1): 24 pp.

- KUTZ, M. 2015. *Mechanical Engineers' Handbook. Volume 1: Materials and Engineering Mechanics*. Wiley.
- LANDOLT, D. 2007. *Corrosion and Surface Chemistry of Metals*. CRC Press.
- LOPESINO, P.; J. ALCÁNTARA; D. DE LA FUENTE; B. CHICO; J.A. JIMÉNEZ; M. MORCILLO. 2018. Corrosion of copper in unpolluted chloride-rich atmospheres. *Metals* 8(11): 866.
- MALVAULT, J.Y.; J. LOPITAU; D. DELAHAYE; M. LENGLET. 1995. Cathodic reduction and infrared reflectance spectroscopy of basic copper (II) salts on copper substrate. *Journal of Applied Electrochemistry* 25: 841–845.
- MARCHAND, G.; E. GUILMINOT; S. LEMOINE; L. ROSSETTI; M. VIEAU; N. STEPHANT. 2014. Degradation of archaeological horn silver artefacts in burials. *Heritage Science* 2: 5.
- MCCAFFERTY, E. 2010. *Introduction to Corrosion Science*. New York: Springer.
- MEIGH, H. 2018. *Cast and Wrought Aluminium Bronzes: Properties, Processes and Structure*. CRC Press.
- MIRCEA, O.; I. SĂRGHIE; I. SANDU; M. QUARANTA; A.V. SANDU. 2009a. The Study of Textile Impressions from Corrosion Products of Some Old Iron Artefacts by Means of the Complementary Analytical Techniques. *Revista de Chimie* 60(2): 201–207.
- MIRCEA, O.; I. SĂRGHIE; I. SANDU; V. URSACHI; M. QUARANTA; A.V. SANDU. 2009b. Study of Some Atypical Degradation Processes of an Iron Archeological Piece. *Revista de Chimie* 60(4): 332–336.
- MONARI, G.; M. GALEOTTI; M. MATTEINI; B. SALVADORI; R. STIFANESE; P. TRAVERSO; S. VETTORI; P. LETARDI. 2023. Protective treatments for copper alloy artworks: preliminary studies of sodium oxalate and limewater effectiveness against bronze disease. *Environmental Science and Pollution Research* 30: 27441–27457.
- NAIR, M.T.S.; L. GUERRERO; O.L. ARENAS; P.K. NAIR. 1999. Chemically deposited copper oxide thin films: structural, optical and electrical characteristics. *Applied Surface Science* 150(1–4): 143–151.
- NAVAL EDUCATION AND TRAINING PROGRAM DEVELOPMENT CENTER (NETPDC). 1972. *Aviation Support Equipment Technician ASE 3 & 2 and ASM 3 & 2. Vol. 1, Basics*. Department of the Navy.
- OUDBASHI, O.; H. FADAEL. 2019. After Eighty Years: Experimental Study of Atmospheric Corrosion in the Metallic Dome of Hafez's tomb, Shiraz, Iran. *Studies in Conservation* 64(4): 208–220.
- OUDBASHI, O.; A. HASANPOUR; P. DAVAMI. 2016. Investigation on corrosion stratigraphy and morphology in some Iron Age bronze alloys vessels by OM, XRD and SEM–EDS methods. *Applied Physics A* 122: 262.
- OUDBASHI, O.; R. NASERI; B. HEIDARPOUR; A. AHMADI. 2019. Study on the Corrosion Mechanisms and Morphology of Archaeological Bronze Objects from a Bronze Age Graveyard in Southwestern Iran. In *Proceedings of the Interim Meeting of the ICOM-CC Metals Working Group (Neuchâtel, Switzerland, September 2-6, 2019)*, eds. C. Chemello, L. Brambilla & E. Joseph, pp. 1–8.
- PAGANO, S.; G. BALASSONE; C. GERMINARIO; C. GRIFA; F. IZZO; M. MERCURIO; P. MUNZI; L. PAPPALARDO; E. SPAGNOLI; M. VERDE; A. DE BONIS. 2023. Archaeometric Characterisation and Assessment of Conservation State of Coins: The Case-Study of a Selection of Antoniniani from the Hoard of Cumae (Campania Region, Southern Italy). *Heritage* 6(2): 2038–2055.
- PETITI, C.; L. TONIOLO; D. GULOTTA; B. MARIANI; S. GOIDANICH. 2020. Effects of cleaning procedures on the long-term corrosion behavior of bronze artifacts of the cultural heritage in outdoor environment. *Environmental Science and Pollution Research* 27: 13081–13094.
- PIETA, E.; J. LEKKI; J.M. DEL HOYO-MELÉNDEZ; C. PALUSZKIEWICZ; M. NOWAKOWSKI; M. MATOSZ; W.M. KWIATEK. 2018. Surface characterization of medieval silver coins minted by the early Piasts: FT-IR mapping and SEM/EDX studies. *Surface and Interface Analysis* 50(1): 78–86.
- REDONDO-MARUGÁN, J.; J. PIQUERO-CILLA; M.T. DOMÉNECH-CARBÓ; B. RAMÍREZ-BARAT; W. AL SEKHANEH; S. CAPELO; A. DOMÉNECH-CARBÓ. 2017. Characterizing archaeological bronze corrosion products intersecting electrochemical impedance measurements with voltammetry of immobilized particles. *Electrochimica Acta* 246: 269–279.
- ROBBIOLA, L.; J.M. BLENGINO; C. FIAUD. 1998. Morphology and mechanisms of formation of natural patinas on archaeological Cu–Sn alloys. *Corrosion Science* 40(12): 2083–2111.
- ROBERTS, B.W.; C.P. THORNTON. 2014. *Archaeometallurgy in Global Perspective: Methods and Syntheses*. Springer.
- SANDU, I.; C. MARUTOIU; I.G. SANDU; A. ALEXANDRU; A. SANDU. 2006. Authentication of old bronze coins I. Study on archaeological patina. *Acta Universitatis Cibiniensis Seria F Chemia* 9(1): 39–53.
- SANDU, I.; O. MIRCEA; A.V. SANDU; I. SARGHIE; I.G. SANDU; V. VASILACHE. 2010. Non-invasive Techniques in the Analysis of Corrosion Crusts Formed on Archaeological Metal Objects. *Revista de Chimie* 61(11): 1054–1058.

- SANDU, I.; N. URSULESCU; I.G. SANDU; O. BOUNEGRU; I.C.A. SANDU; A. ALEXANDRU. 2008. Pedological stratification effect of corrosion and contamination products on Byzantine bronze artefacts. *Corrosion Engineering, Science and Technology* 43(3): 256–266.
- SANDU, I.G.; F.A. TENCARIU; D.M. VORNICU; A.V. SANDU; A. VORNICU; V. VASILACHE; I. SANDU. 2014. Establishing the archaeo-metallurgic ornamentation process of an axe from the bronze age by OM, SEM-EDX, and Micro-FTIR. *Microscopy Research and Technique* 77(11): 918–927.
- SCOTT, D.A. 1994. An Examination of the Patina and Corrosion Morphology of Some Roman Bronzes. *Journal of the American Institute for Conservation* 33(1): 1–23.
- SCOTT, D.A. 1997. Copper compounds in metals and colorants: Oxides and hydroxides. *Studies in Conservation* 42(2): 93–100.
- SCOTT, D.A. 2002. *Copper and Bronze in Art: Corrosion, Colorants, Conservation*. Los Angeles: Getty Publications.
- SCOTT, D.A. 2011. *Ancient Metals: Microstructure and Metallurgy*. Vol. 1. Los Angeles: Conservation Science Press.
- STRANDBERG, H. 1998. Reactions of copper patina compounds—I. Influence of some air pollutants. *Atmospheric Environment* 32(20): 3511–3520.
- STRANDBERG, H.; L.G. JOHANSSON. 1998. Some Aspects of the Atmospheric corrosion of copper in the presence of sodium chloride. *Journal of the Electrochemical Society* 145(4): 1093.
- THYSSEN INC. 1998. *Bronze Alloys: A Comparative Guide to Alloys, Applications and Availability*. Thyssen, Copper and Brass Sales.
- TORRISI, L.; F. CARIDI; L. GIUFFRIDA; A. TORRISI; G. MONDIO; T. SERAFINO; M. CALTABIANO; E.D. CASTRIZIO; E. PANIZ; A. SALICI. 2010. LAMQS analysis applied to ancient Egyptian bronze coins. *Nuclear Instruments and Methods in Physics Research Section B: Beam Interactions with Materials and Atoms* 268(10): 1657–1664.
- VASSILIOU, P.; O. PAPADOPOLOU; S. GRASSINI; E. ANGELINI. 2019. Provenance, manufacturing and corrosion behavior of Ancient Hellenistic coins from Egypt. In *2019 IMEKO TC4 International Conference on Metrology for Archaeology and Cultural Heritage*, pp. 554–559.
- VOLPI, F.; M. VAGNINI; R. VIVANI; M. MALAGODI; G. FIOCCO. 2023. Non-invasive identification of red and yellow oxide and sulfide pigments in wall-paintings with portable ER-FTIR spectroscopy. *Journal of Cultural Heritage* 63: 158–168.
- WANG, Y.; Y.X. MOO; C. CHEN; P. GUNAWAN; R. XU. 2010. Fast precipitation of uniform CaCO₃ nanospheres and their transformation to hollow hydroxyapatite nanospheres. *Journal of Colloid and Interface Science* 352(2): 393–400.
- WANG, X.; J. SONG; H. ZHOU; Z. FAN; J. SHI; J. CHEN; K. XIAO. 2023. Mechanism of dendrite segregation on corrosion behaviour of antique cast low Sn bronze. *Corrosion Science* 222: 111402.
- WU, J.; J. WANG. 2019. The effects of UV and visible light on the corrosion of bronze covered with an oxide film in aqueous solution. *Corrosion Science* 154: 144–158.
- YANG, Y.; X. CAO; Y. LI; Z. WANG; B. LI; X. JIANG; J. JIA; C. PAN. 2020. Spontaneous Symmetry-Breaking in the Corrosion Transformation of Ancient Bronzes. *Minerals* 10(8): 656.
- YU, P.; R.J. KIRKPATRICK; B. POE; P.F. McMILLAN; X. CONG. 1999. Structure of Calcium Silicate Hydrate (C-S-H): Near-, Mid-, and Far-Infrared Spectroscopy. *Journal of the American Ceramic Society* 82(3): 742–748.